GA–A22638

SCALING OF ELM AND H–MODE PEDESTAL CHARACTERISTICS IN ITER SHAPE DISCHARGES IN THE DIII–D TOKAMAK

by

T.H. OSBORNE, R.J. GROEBNER, L.L. LAO,
A.W. LEONARD, R. MAINGI,[1] R.L. MILLER,
G.D. PORTER,[2] D.M. THOMAS, and R.E. WALTZ

JULY 1997

GA–A22638

SCALING OF ELM AND H–MODE PEDESTAL CHARACTERISTICS IN ITER SHAPE DISCHARGES IN THE DIII–D TOKAMAK

by

T.H. OSBORNE, R.J. GROEBNER, L.L. LAO,
A.W. LEONARD, R. MAINGI,[1] R.L. MILLER,
G.D. PORTER,[2] D.M. THOMAS, and R.E. WALTZ

This is a preprint of a paper presented at the 24th EPS Conference on Controlled Fusion and Plasma Physics, June 9–13, 1997, Berchtesgaden, Germany, and to be printed in the *Proceedings.*

Work supported by U.S. Department of Energy
Contracts DE-AC03-89ER51114, DE-AC05-96OR22464,
and W-7405-ENG-48

[1]Oak Ridge National Laboratory
[2]Lawrence Livermore National Laboratory

GENERAL ATOMICS PROJECT 3466
JULY 1997

SCALING OF ELM AND H–MODE PEDESTAL CHARACTERISTICS IN ITER SHAPE DISCHARGES IN THE DIII–D TOKAMAK*

T.H. Osborne and the DIII–D H–mode Pedestal Study Group: R.J. Groebner, L.L. Lao, A.W. Leonard, R. Maingi,† R.L. Miller, G.D. Porter,‡ D.M. Thomas, and R.E. Waltz

General Atomics, P.O. Box 85608, San Diego, California 92186-9784, U.S.A.

1. Introduction

A defining feature of H–mode is the existence of a transport barrier near the plasma boundary. Although the H–mode edge transport barrier can be quite narrow (in DIII–D $\leq 2\%$ of the minor radius), the characteristics of this layer are significant in the overall plasma performance and in divertor effects.

Stiff ITG-mode turbulent transport models [1,2] predict that the core transport coefficients are reduced strongly with increasing edge temperature suggesting that ITER may require relatively high edge temperature for ignition. This result is in qualitative agreement with data from DIII–D and C-MOD [3]. On DIII–D, H-ITER93-H $\propto (T_e^{PED})^{0.55} (n_e^{PED})^{0.58}/B_T^{0.93}$, where H-ITER93-H is the energy confinement enhancement factor relative to ITER H–mode scaling, and PED refers to values at the top of the H–mode pedestal (Fig. 1). The periodic collapse of the pressure gradients associated with the H–mode transport barrier at ELMs is important not only in setting the average H–mode pedestal height, but also the short time scale of the ELM energy loss can result in large power loads to the divertor plates in ITER.

This paper primarily describes experiments in DIII–D employing discharges with ITER cross-sectional shape and aspect ratio ($L_{DIII-D}/L_{ITER} = 0.2$, where L is the length scale). In these experiments, the plasma current and toroidal field were varied by a factor of two as was the q, $3 < q_{95} < 6$, where $q_{ITER} \cong 3$. The neutral beam heating power was varied over the range $0.06 < P/S$ (MW/m^2) < 0.3, where 0.17 (IGNITION) $< P/S_{ITER} < 1.25$ (BURN), where P is the loss power, S is plasma surface area, and the density was in the range $0.2 < n_G = n / n_{GREENWALD} < 0.7$, while $n_{G-ITER} \approx 1.0$. These were gas puff fueled discharges in an open divertor configuration, with no divertor pumping, and the ∇B drift toward the x–point.

2. Scaling of H–mode Pedestal Parameters

We separated our study of the H–mode pedestal parameters into analysis of the scaling of the width of the steep pressure gradient region, which is expected to be set by turbulence suppression physics [4], and the magnitude of the gradient, which may be limited by the ELM instability [5].

The width of the H–mode transport barrier used in the scaling studies is determined from Thomson scattering measurements of the electron pressure profile which are fit to a hyperbolic tangent functional form in the edge region. We find that the width of the edge

*Work supported by U.S. Department of Energy Contracts DE-AC03-89ER51114, DE-AC05-96OR22464, and W-7405-ENG-48.

†Oak Ridge National Laboratory, Oak Ridge, Tennessee.

‡Lawrence Livermore National Laboratory, Livermore, California.

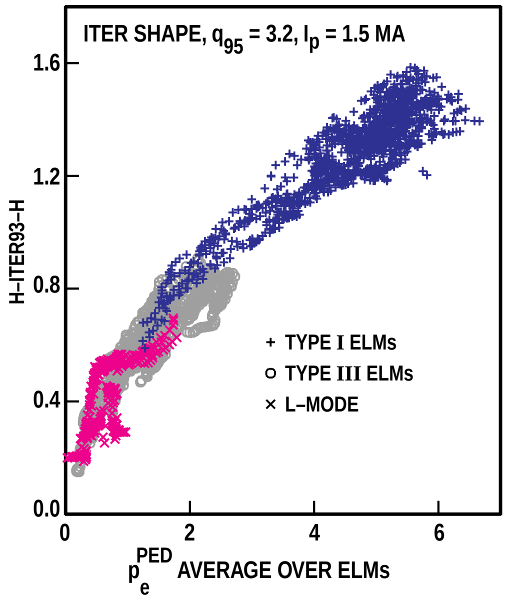

Fig. 1. H–mode energy confinement enhancement factor relative to ITER93-H–mode scaling increases with increasing H–mode pedestal pressure (kPa) averaged over ELMs.

steep gradient region for the ion pressure generally matches that of the electrons. Parameters that were available for fitting included the electron profile parameters, and MHD equilibrium parameters which are determined from external magnetic measurements using the EFIT code. The width scaling relations presented here apply to the interval between type I ELMs; during type I ELMs the width expands greatly. Only p_e^{PED}, T_e^{PED}, and B_{pol} had significant correlation with the transport barrier width. Because of a correlation between density and plasma current, the width of the steep gradient region on the outboard midplane could be fit equally well to the edge pressure, $\delta \propto (p_e^{PED})^{0.52} / \langle B_{pol} \rangle^{0.94}$ (Fig. 2) or edge temperature, $\delta \propto (T_e^{PED})^{0.36} / \langle B_{pol} \rangle^{0.44}$. In dimensionless variables, the normalized width was equally well fit to the a power of the poloidal gyroradius, $\delta/R \propto (\rho_{POL}/R)^{0.66}$, or to the edge β_{POL}, $\delta/R \propto (\beta_{POL}^{PED})^{0.4}$. For low density type III ELMs (described in Section 2) the width is 20% to 50% larger than for type I even though p_e^{PED} and T_e^{PED} are typically signifcantly smaller. For low temperature type III ELMs the width appears to be similar to the type I case, although an explicit scaling has not been derived.

In the ITER shape discharges on DIII–D, we find that the electron pressure gradient normalized as for ballooning mode stability, $\alpha_{MHD} = 2\mu_0 (dp_e/d\psi)(dV/d\psi)[V/(2\pi^2 R)]^{1/2}/4\pi^2$ before a type I ELMis relatively constant and independent of q (Fig. 3). This is in contrast to $\alpha_{CYL} = 2\mu_0 (dp_e/dR)(q_{95}/B)^2 R$ which rises sharply at low s/q^2 (where s is the magnetic shear), and increases with increasing input power at high q. This behavior of α_{CYL} does not necessarily suggest second stability, instead it may be understood from the fact that $\alpha_{CYL}/\alpha_{MHD} \cong q_{95}/q_{LOCAL}$, where q_{LOCAL} is the local q on the outboard midplane, and q_{95}/q_{LOCAL} increases with increasing β_{pol}. Using MHD equilibria determined from external magnetic measurements, we computed the stability to ideal, infinite n,

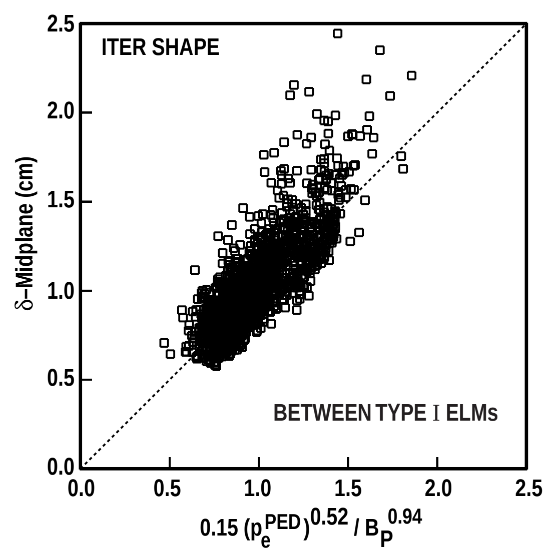

Fig. 2. Width of the H–mode steep gradient region on the outboard midplane between type I ELMs fit to powers of the electron pressure pedestal height, p_e^{PED} (kPa), and the surface averaged poloidal field B_p (T).

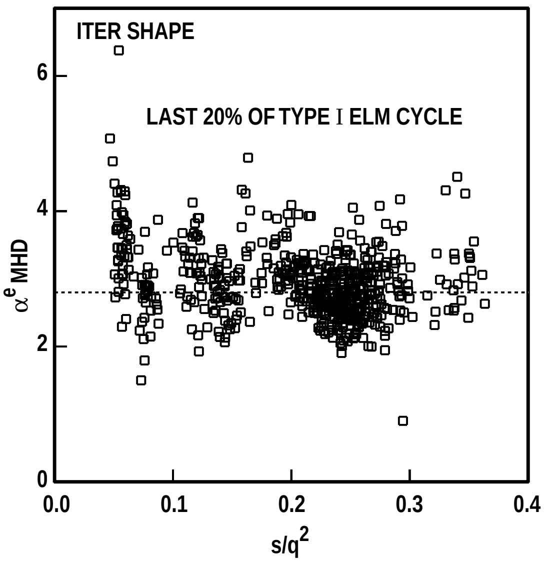

Fig. 3. Edge electron pressure gradient normalized as for ballooning mode stability just before a type I ELMs is relatively independent of s/q^2 *where* s *is the magnetic shear.*

ballooning modes with the BALOO [6] code. The electron pressure alone was found to be equal to or greater than the predicted first stable limit. In the few cases where the ion temperature was determined, it was similar to the electron temperature so that the experimental pressure gradient is expected to exceed the first stable limit by roughly a factor of two. Preliminary work indicates that self consistently adding the current density expected to be associated with the edge pressure gradient does not significantly change the first stable limit, however local regions of second stable access can be created in regions of high pressure gradient if the current is large enough to reduce s/q^2 below a critical value. Since s/q^2 generally decreases with increasing minor radius in these discharges, this mechanism might limit the width of the high pressure gradient region at a point where the pressure gradient is less than its peak value.

We can estimate the edge temperature in ITER by assuming type I ELMs will occur at the same α as in DIII–D at ITER q. Scaling from DIII–D discharges, $\delta/R \propto (\rho_{\mathrm{POL}}/R)^{2/3}$ gives $T^{\mathrm{PED}} \propto (LB_{\mathrm{T}}/n_{\mathrm{G}}^3)^{1/2} \approx 1$ keV for ITER [this scaling also implies $\delta \propto (L/n_{\mathrm{G}}B_{\mathrm{T}})^{1/2}$,ß and $p^{\mathrm{PED}} \propto (B_{\mathrm{T}}^3/n_{\mathrm{G}}L)^{1/2}$). For $\delta/R \propto (\beta_{\mathrm{POL}}^{\mathrm{PED}})^{1/2}$, $T^{\mathrm{PED}} \propto (LB_{\mathrm{T}}/n_{\mathrm{G}}) \approx 5$ keV for ITER (and here $\delta \propto L$, and $p^{\mathrm{PED}} \propto B_{\mathrm{T}}^2$).

3. ELM Classification, Energy Loss, and Divertor Effects

Type I, II, and III ELMs [7] were observed in the ITER shape discharges on DIII–D. Type I and III ELMs appeared in distinct regions of $n_{\mathrm{e}}^{\mathrm{PED}}$, $T_{\mathrm{e}}^{\mathrm{PED}}$ space (Fig 4). Type II ELMs were interspersed with type I ELMs and became more prevalent at high β_{POL} although they never replaced type I ELMs.

The energy lost from the plasma core during type I ELMs was determined from the time history of the stored energy obtained from MHD equilibrium. Data from DIII–D was combined with a few points from ASDEX-U and JET to produce a scaling for the type I ELM energy loss, $\Delta E_{\mathrm{ELM}}/E_{\mathrm{TOTAL}} \propto (P/S)^{-0.4} B^{-0.3}$ where P is the total input power and S is the plasma surface area, which gives $\Delta E_{\mathrm{ELM}} \cong 26$ MJ for ITER. We can also estimate ΔE_{ELM} in ITER by assuming that the change in normalize pressure gradient, α, will be the same as that observed in DIII–D and that the pressure drops equally across the cross-section. For $\delta/R \propto (\rho_{\mathrm{POL}}/R)^{2/3}$, $\Delta E_{\mathrm{ITER}} \approx 7$ MJ, while for $\delta/R \propto (\beta_{\mathrm{POL}}^{\mathrm{PED}}/R)^{1/2}$, $\Delta E_{\mathrm{ITER}} \approx 37$ MJ. IR camera measurements indicate that 75% to 100% of ΔE_{ELM} reaches the divertor plates on a time scale of 1–2 ms, with about twice as much going to the inboard relative to the outboard strike point. The ELM heat flux is distributed over roughly a factor of two larger area in the

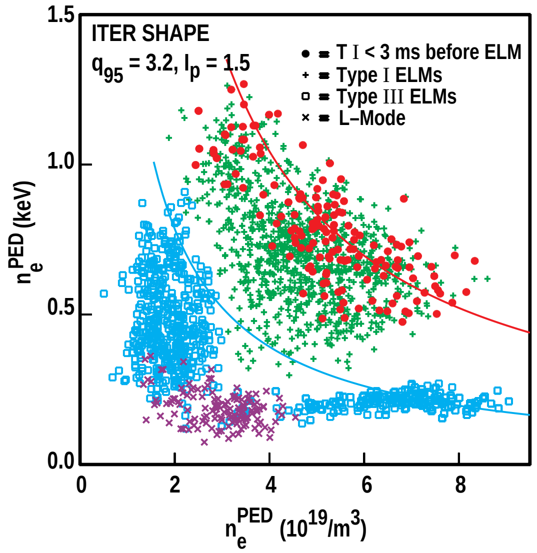

Fig. 4. Different classes of ELMs appear in distinct regions of $n-T$ space. Two different classes of type III ELMs appear at low temperature and low density (pressure gradient). Solid curves are constant pressure.

divertor than the steady-state heat flux. Bolometry indicates that less than about 5% of ΔE_{ELM} is radiated.

Two distinct classes of type III ELMs were identified. One class, which has been studied extensively on ASDEX-U [7], occurs below a critical edge temperature, and may be compatible with high H factor at high density where p^{PED} is comparable to that for type I ELMs. A second class of type III ELMs was identified at low density. These ELMs disappear above a critical heating power which scales as $I_p^{2.4}/n_e^2$, or, in terms of local quantities, when the edge pressure gradient is ablve a critical value which scales as I_p^2. Possibly because of this limitation on edge pressure gradient the H–mode pedestal and energy confinement is reduced in discharges with low density type III ELMs, typically $0.6 <$ H-ITER93-H < 0.9. This may be of concern since these ELMs can occur at powers near the H–mode threshold power if the density, or perhaps neutral pressure, is low enough.

4. Conclusions

We have shown a correlation between the H–mode pressure pedestal height and the energy confinement enhancement in ITER shape discharges on DIII–D which is consistent with the behavior of H in different ELM classes. The width of the steep gradient region was found to equally well fit the scalings $\delta/R \propto (\rho_{POL}/R)^{2/3}$ and $\delta/R \propto (\beta_{POL}^{PED}/R)^{1/2}$. The normalized pressure gradient α_{MHD} was found to be relatively constant just before a type I ELM. An estimate of T^{PED} for ITER gave 1 to 5 keV. We also estimate $\Delta E_{ELM} \cong 26$ MJ for ITER. We identified a distinct class of type III ELM at low density which may play a role in setting H at powers near the H–mode threshold power.

5. References

[1] M. Kotschenreuter *et al*,, Proc. 16th Int. Conf. on Plasma Phys. and Contr. Nucl. Fusion Res., Montréal (1996), IAEA-F1-CN-64/D1-5.
[2] R.E. Waltz *et al*., *Proc*. 16th Int. Conf. on Plasma Phys. and Contr. Nucl. Fusion Res., Montréal (1996), IAEA-F1-CN-64/D1-6.
[3] A. Hubbard *et al*., Proc. 16th Int. Conf. on Plasma Phys. and Contr. Nucl. Fusion Res., Montréal (1996), IAEA-F1-CN-64/D1-6.
[4] K.H. Burrell *et al*., Plasma Phys. and Contr. Fusion **34**, 1859 (1992).
[5] P. Gohil *et al*., Phys. Rev. Lett. **61**, 1603 (1988).
[6] R.L. Miller *et al*., Phys. Plasmas **4**, 1062 (1997).
[7] H. Zohm, Plasma Phys. and Contr. Fusion **38**, 105 (1996).